3D Force Prediction Using Fingernail Imaging with Automated Calibration

Thomas Grieve*
Department of Mechanical Engineering
University of Utah

Lucas Lincoln†
Department of Mechanical Engineering
University of Utah

Yu Sun‡
Department of Computer Science and Engineering
University of South Florida

John M. Hollerbach§
School of Computing
University of Utah

Stephen A. Mascaro¶
Department of Mechanical Engineering
University of Utah

ABSTRACT

This paper demonstrates a system for 3D force prediction using fingernail imaging, in which video images of the human fingernail are used to predict the normal and shear forces that occur when the finger is in contact with a flat surface. The automated calibration uses a magnetic levitation haptic device (MLHD) whose flotor has been modified to apply forces to the human fingerpad.

The system accurately predicts forces with an RMS error of 0.3N normal force, 6% of the full range of 10N, and a shear force error of 0.3N, 3% of the full range of $\pm$2.5N. This paper also demonstrates that varying the number of pixels used to represent the finger between 100 and 500 pixels has little effect on the results, indicating that a real-time application could use low-resolution images without loss of accuracy.

1 INTRODUCTION

Fingernail imaging as a means of estimating the level of force on a human finger was first proposed by Mascaro and Asada in [7]. The concept of fingernail imaging is based on the movement of blood in the tissue underlying the fingernail. As the fingerpad interacts with surfaces, blood pools in certain regions and flees from others. This results in a coloration change in the tissue beneath the fingernail, which is essentially transparent. This paper presents a method of automatically calibrating the fingernail imaging system over the useful 3D force space. As prior imaging calibration methods rely on user input and only calculate force on one axis at a time, this new calibration procedure results in a more robust model that is better able to predict arbitrary combinations of normal and shear force.

In [7], a fingernail sensor designed to detect this coloration effect was introduced. The sensors are mounted on the test subject's fingernail and consist of an array of LEDs to illuminate the fingernail and photodetectors to measure the coloration effect. The coloration information allows calibration of a model, which leads to the prediction of forces. The original research found that force magnitude and direction could be predicted over a range of shear forces up to 2N with an error of 0.5N and normal force up to 3N with an error of 1N. It was later demonstrated in [8] that the fingernail coloration response exhibits common patterns across all people. This justifies the use of this method to detect finger force. Detecting force in this way has a wide range of potential applications. For example, computer input devices such as a keyboard or mouse could be completely replaced by a finger force detection system using an attached camera. The detection method can also be used to study grasping forces in a variety of environments.

The on-nail sensor approach suffers from two major problems. First, the sensors must be custom manufactured to fit each test subject. Second, and perhaps more important, the resolution of these sensors is limited by the number of photodetectors and LEDs that can be imbedded into the sensors. An attempt to overcome these difficulties was made in [11], wherein the fingernail was imaged by a high-resolution digital camera. This provides a much larger data set while eliminating the need for customization. Using this new method, the error was reduced to 0.3N over a range of normal force up to 10N. In later experiments, force magnitude was predicted in one direction at a time with an accuracy of 0.1N over the range of normal force up to 10N and shear force up to 2N [13]. It was demonstrated in [14] that discrete finger force directions could be predicted with an accuracy of 90% without any individual calibration. This prediction accuracy held steady as the resolution of the images was decreased to 10×10 pixels. The major limitations of finger force prediction using a digital camera are the need for consistent lighting and the requirement that the fingernail remain in view of the camera. Future work will investigate solutions to these problems so that the method can be used in a wide variety of environments.

A major challenge for both methods of imaging is the need for calibration. In the past, this has occurred mainly using user-supplied forces. The test subject was presented with a force sensor mounted on a frame and asked to apply forces to explore the space for calibration. As in [9], guidance through the force space is provided by a GUI that shows a target force as a circle whose radius is proportional to the normal force, while the (x,y)-position of the center of the circle represents the shear forces (f_x, f_y). The test subject is asked to apply forces to the sensor so that a second circle matches the target circle. One limitation of this method is the time required for the test subject to become familiar with the interface to the extent that they can follow the target. A second drawback is that the user becomes fatigued after a time, which places a limit on the number of images that can be recorded in a given sitting. Third, it is difficult for a human to consistently control these three variables. These problems will be amplified as it is eventually desired to include shear torque, fingerpad contact angle with the sensor and finger joint angles. As such, an automated calibration system is desired which will allow the test subject to remain passive while the calibration occurs. This would reduce the fatigue, allowing for more time in the calibration. Additionally, the images can be collected more rapidly, as the speed of the controller can be set much higher than that achievable by a human controlling the finger. Finally, the controller could be augmented to control other variables of interest, allowing more detailed calibration to occur.

In [5], a controller designed to apply forces to the human fingerpad using a 6-DOF magnetic levitation haptic device (MLHD) was designed. This controller, in a modified form, provides the basis for the automated calibration procedure detailed herein. The

*e-mail: tom.grieve@utah.edu
†e-mail:lucas.lincoln@utah.edu
‡e-mail:yusun@cse.usf.edu
§e-mail:jmh@cs.utah.edu
¶e-mail:smascaro@mech.utah.edu

IEEE Haptics Symposium 2010
25 - 26 March, Waltham, Massachusetts, USA
978-1-4244-6822-5/10/$26.00 ©2010 IEEE

main purpose of this paper is to detail the methods and present the results of this automated calibration. Section 2 details the experimental setup, while section 3 explains how the data analysis was performed. Section 4 compares the effectiveness of different registration methods. Section 5 demonstrates the successful implementation of this calibration method and the results of predicting force using this method.

2 Calibration Setup

To use fingernail imaging as a means of detecting fingerpad force levels, individual calibration is necessary. Automated calibration can be performed using the MLHD developed by Hollis [1]. With this method, the test subject is asked to relax while the MLHD is controlled to exert force on the subject's fingerpad. This has the dual benefits of allowing the data collection to proceed more rapidly while simultaneously limiting the exertion required by the test subject. In this way a much larger data set can be collected than would be possible otherwise, allowing for the formation of a more detailed model.

During calibration, the test subject is seated in front of the MLHD. An armrest with an adjustable finger restraint is used to guide the subject's finger to the correct location and posture. The camera is mounted over the MLHD flotor using an adjustable microphone extender, which allows the camera to be repositioned for each test subject. A lighting dome is placed over the camera to provide consistent, indirect lighting between tests. The dome has several white LEDs mounted such that they provide diffuse lighting over the finger. A light shield covers the MLHD during tests to eliminate the effects of ambient light. The setup is illustrated in Figure 1.

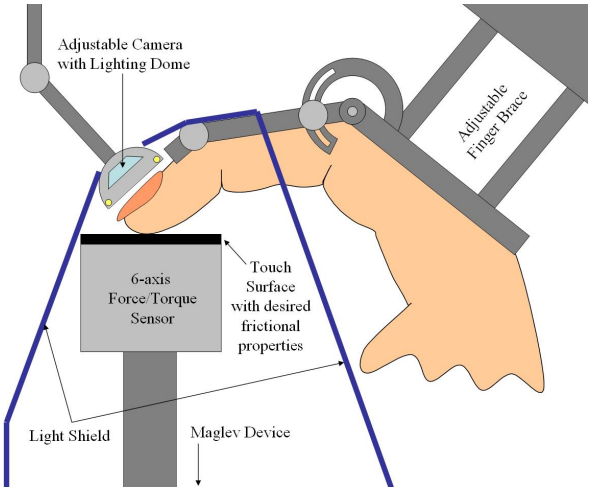

Figure 1: Illustration of Calibration Setup

Data was collected from 16 test subjects. The subjects include both males and females. The subjects range in age from early 20s to late 50s. Each subject was asked to sit in the testing apparatus, as shown in Figure 2, while they were introduced to the MLHD and the purpose of the calibration. A sample trajectory was run without the light shield to allow the test subject to see what happens during a test and for the experimenter to verify that everything is performing as desired. Then the light shield was put in place and several test trajectories were run on each subject.

The controller developed in [5] has been modified as shown in Figure 3. The MLHD is now controlled using pure force control. The input signal is calculated using a PIV force controller, as in [10]. This signal is sent to the MLHD server as a force command. This improves the step response as shown in Figure 4, as well as the

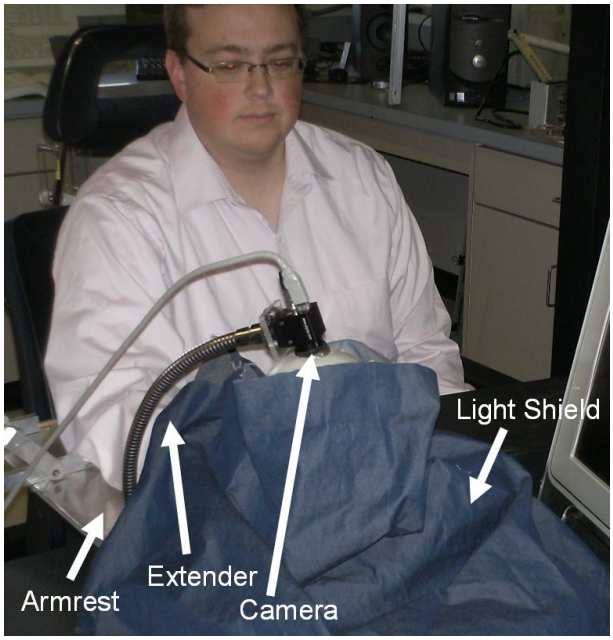

Figure 2: Calibration setup

disturbance rejection performance. The system still requires almost 0.2 seconds to dampen the vibrations in the unchanging directions. However, as the intended trajectories will use ramps rather than steps, this effect is not seen during normal operation.

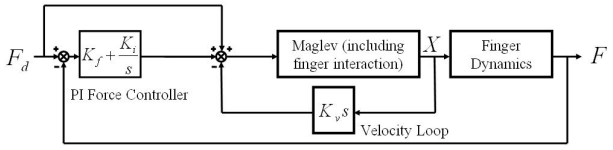

Figure 3: New force controller for automated calibration

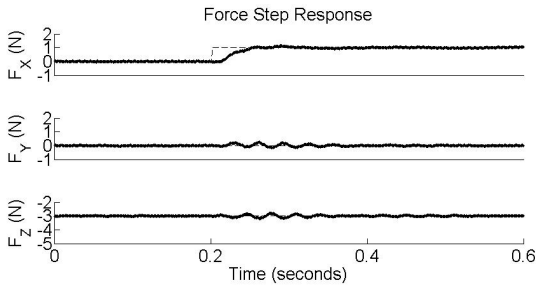

Figure 4: Force response of new controller

It is desired that the calibration routine fully explore the useful force space for the coloration effect. This force space includes normal force up to 10N and shear force up to 5N. The test trajectories that have been selected vary the method used to cover the conical force space in several different ways. Some use a Cartesian (x-y-z) grid overlaid on the cone, while others use cylindrical (r-θ-z) grids. These are illustrated in Figure 5. The minimum distance between adjacent points on the grid, ΔF, is varied between 0.125N and 0.5N. The slope of the edge of the cone is varied between 0.25 and 0.67. Some trajectories cover the entire cone while others only

cover the lower ($0\text{N} \leq f_n < 4\text{N}$), middle ($4\text{N} \leq f_n < 7\text{N}$) or upper ($7\text{N} \leq f_n \leq 10\text{N}$) portions. Additionally, some specialty trajectories only apply z-direction forces, while others only apply shear force in one direction (i.e., $f_y = 0$ or $f_x = 0$). 28 different trajectories have been designed for use. Each trajectory contains between 30 and 800 target force levels. However, due to time constraints and fatigue, only a few of these trajectories can be applied to any given test subject in one sitting. Trajectories are selected at random for each test subject. Thus, several hundred (and in most cases a few thousand) images can be collected for each test subject in a single 30-minute training period.

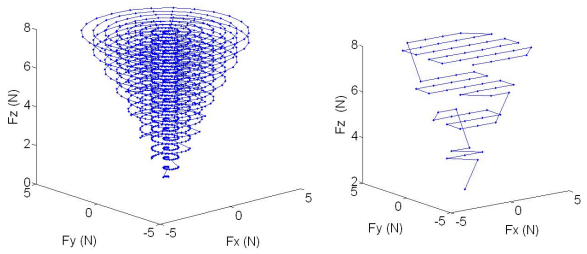

Figure 5: Sample trajectories of the type used in calibration. Left: Cylindrical Grid. Right: Cartesian Grid.

Within a given trajectory, each force level is held for 0.4 seconds. During this time the camera records an image at a resolution of 1024×768 pixels. As part of this process, the (f_x, f_y, f_z) values recorded by the force sensor are stored in the (R, G, B) indices of pixel $(1,1)$ of the image. The range of forces to be recorded is:

$$\begin{aligned} -5.0\text{N} \leq f_x \leq 5.0\text{N} \\ -5.0\text{N} \leq f_y \leq 5.0\text{N} \\ -10.0\text{N} \leq f_z \leq 0.0\text{N} \end{aligned}$$

Each force direction has a possible range of 10N. A margin of error of 1N is added to each end of the above ranges, giving a possible range of 12N. Each color channel can store an integer between 0 and 255. Thus, the forces are encoded using the following formulas:

$$\begin{aligned} R &= \text{floor}(21.25(f_x + 6)) \\ G &= \text{floor}(21.25(f_y + 6)) \\ B &= \text{floor}(21.25(1 - f_z)) \end{aligned} \quad (1)$$

So, $f_x = 0.0\text{N}$ corresponds to $R = 127$, while $f_z = -5.0\text{N}$ results in $B = 127$. This has the advantage of not requiring an additional file to store the force data, while maintaining required precision. The error in recording the force using this encoding is at most $1/21.25 = 0.047N$, which is an order of magnitude below the minimum level of distinguishable error previously established using fingernail imaging (0.3N).

3 Data Analysis

Once the images have been collected, Matlab is used to process them. First, each image is registered to a target image. Second, the force and intensity information are extracted from each image. Finally, the least squares method is used to form a model from all of the images.

Since the finger moves during the calibration procedure, it is necessary to register each image to a target image. The target chosen for each data set is the first image taken from that test subject. The process of registration is discussed in section 4.

The recorded force information is decoded from each image using the inverse of Equations 1. These values are stored as the force vector **f**:

$$\mathbf{f} = \begin{bmatrix} f_x \\ f_y \\ f_z \end{bmatrix} = \begin{bmatrix} \frac{R}{21.25} - 6 \\ \frac{G}{21.25} - 6 \\ 1 - \frac{B}{21.25} \end{bmatrix} \quad (2)$$

As the number of pixels is extremely large and the changes in intensity correlate with position, the registered images are subdivided into cells of a specified size. Additionally, it has been found that the green channel is most sensitive to changes in force [11], so the other channels are discarded and only the green-channel intensity values of all pixels in each cell are averaged. The results are stored in the pixel vector **p**:

$$\mathbf{p} = \begin{bmatrix} p_1 \\ p_2 \\ \vdots \\ p_m \end{bmatrix} \quad (3)$$

The force is assumed to be a linear combination of the cell intensities:

$$\begin{aligned} f_x &= a_0 + a_1 p_1 + a_2 p_2 + \cdots + a_m p_m \\ f_y &= b_0 + b_1 p_1 + b_2 p_2 + \cdots + b_m p_m \\ f_z &= c_0 + c_1 p_1 + c_2 p_2 + \cdots + c_m p_m \end{aligned}$$

This results in the following matrix equation:

$$\begin{bmatrix} f_x \\ f_y \\ f_z \end{bmatrix} = \begin{bmatrix} a_0 & a_1 & a_2 & \cdots & a_m \\ b_0 & b_1 & b_2 & \cdots & b_m \\ c_0 & c_1 & c_2 & \cdots & c_m \end{bmatrix} \begin{bmatrix} 1 \\ p_1 \\ p_2 \\ \vdots \\ p_m \end{bmatrix}$$

$$\mathbf{f} = \mathbf{A}\mathbf{p}$$

$$\mathbf{A} = \begin{bmatrix} a_0 & a_1 & a_2 & \cdots & a_m \\ b_0 & b_1 & b_2 & \cdots & b_m \\ c_0 & c_1 & c_2 & \cdots & c_m \end{bmatrix}$$

The transpose is taken and the equations for each image are stacked, to form the final least squares equation. This is solved for the coefficient matrix **A**. These values can be used to test the model.

3.1 Model Verification

The first test for the model, training, is to determine how well the data fits the model. This is done by applying the model to each of the training images in turn and calculating the predicted force. This is then compared to the actual force measured when the image was recorded. The total RMS error for the data set is calculated. This is the equivalent of finding the error with which a straight line fits a set of (x,y) data.

The second test for the model, validation, is to determine how well the model fits an image that was not used to form the model. To accomplish this, an image is removed from the data set. A model is formed using the remaining data. This model is then applied to the removed image and a predicted force is calculated. This is compared to the actual force measured when the image was recorded. Again, the total RMS error for the data set is calculated.

The results of these two tests will be discussed in detail in Section 5. First, an investigation into different registration methods is presented.

4 REGISTRATION

Fingernail locations vary in the image frame as the MLHD applies shear and normal forces to the finger. As a particular fingernail is imaged, it is necessary to register all points on each image to a common reference. Successful registration directly influences the accuracy of the force prediction, as well as its repeatability.

The fingernail is a relatively featureless item, making robust, accurate registration somewhat difficult. Adding to this difficulty is the varying intensities which result from the testing itself, as image registration techniques rely on intensity measurements across image sets. In other words, the variations of interest (pixel intensity changes) must be preserved while correcting for movement and distortions [2].

Three registration techniques are explored: A Harris feature point detection algorithm, a Canny edge detection algorithm and an affine rigid body transformation method. The former two cases are used in conjunction with random sample consensus (RANSAC) model fitting [4].

4.1 Methods

4.1.1 Harris

The Harris feature detection system [6] is used to detect corner points by first smoothing the image using a Gaussian filter, computing the gradients isotropically and finding local gradient maxima. An example image is shown in Figure 6(a), which shows the finger imaged in the MLHD test setup during a data collection with detected feature points indicated by plus signs.

The Harris algorithm is used to find feature points in the first image and then in each successive image. As each image is processed, the neighborhoods of and distances between feature points on the first image and the current image are compared to determine matching feature points (Figure 6(b)). Once this correlation has taken place, RANSAC is performed to determine the transformation model. The inliers found using RANSAC are shown in Figure 6(c). The current image is then transformed so that it aligns with the first image.

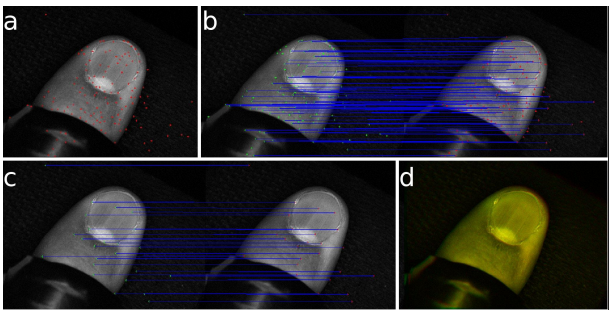

Figure 6: Illustration of the Harris method. (a) The reference image showing feature points as small + signs. (b) Harris feature points with correlated points connected by lines. (c) RANSAC inliers connected by lines. (d) Image for qualitative inspection after transformation.

A qualitative check for each technique is to create a new image consisting of a red and green color channel, the red channel being supplied from the reference image intensities, and the green channel from the transformed image intensities. In Figure 6(d), a quality image registration is evidenced by the lack of ghost images. Comparatively, a ghost image is evidence that the images are not successfully registered. Figure 7 demonstrates this poor registration, where the image transformed does not successfully overlay the reference image, evidenced by the ghost image along the left side of the finger.

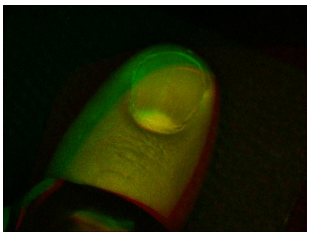

Figure 7: Poor image registration

4.1.2 Canny

In the hope that fingernails may be better defined by edges rather than feature points, a Canny edge detection algorithm [3] was implemented for registration. Again based on gradient detection, the Canny algorithm detects edges by thresholding the gradient at a high and a low level to produce two binary images. The high-thresholded image is used to begin tracing edges, and the low-thresholded image is used to fill in the gaps in these edges as needed.

Similar to the Harris process, once the edge data is determined for the reference image and the image currently being registered, the edges are matched by correlation by a simple comparison of distance. This data is passed to RANSAC to determine inliers and subsequent transformation. Figure 8 shows the four steps of the Canny registration process.

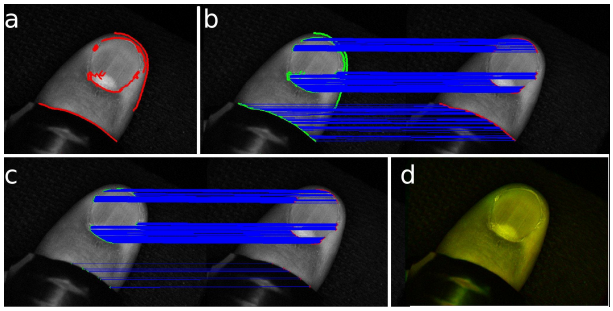

Figure 8: Illustration of the Canny method

4.1.3 Scaled Rigid-Body Transform

The fingernail perspective is typically consistent, particularly during the calibration procedure discussed previously, suggesting that a combination of linear translation, rotation and scaling can successfully register a set of images. Generally, the MLHD introduces small translations in the X and Y shear directions and small changes in scale via Z normal forces. A rigid-body transformation was developed to register the nail images according to these assumptions. A similar method was used for registration in [12].

To implement this technique, a binary image is created by intensity thresholding the image in question. This binary image is morphologically opened to eliminate all small areas, as the largest area corresponds to the finger with the MLHD and camera setup. The major axis of the finger is computed from the binary image to correct for rotations. After rotation, the bounding box of the finger image is used as a rudimentary foreground/background isolation to separate the finger from the image background. The images are cropped to the finger bounding box, and scaled to fit the reference image finger dimensions. This is illustrated in Figure 9.

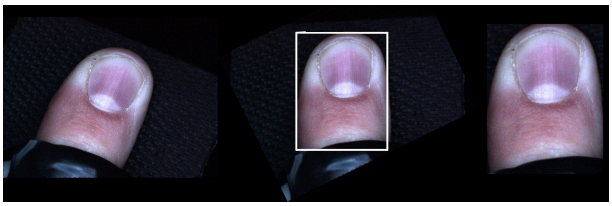

Figure 9: Illustration of the Rigid Body Transformation method

4.2 Evaluation of Registration Methods

For our immediate work, it is required that the registration be accurate when registering images taken in the MLHD/Camera setup and this accuracy is the primary focus of evaluation. Additionally, reducing computation time is desirable now (as a large foundation of data is being gathered and analyzed) and in the future (for real time implementation). A robust method is desirable for future real-environment application (with varying lighting conditions and finger orientation). With these considerations in mind, the registration techniques were evaluated for use with this project.

To determine the accuracy of the registration, data sets were registered with each method. A model was built to the image data and force readings and the validation results were compared. More details on the analysis procedure, including validation, are discussed in Section 3 of this paper.

Given the same set of images, force readings and optimized parameters for model fitting and validation, the RMS error difference in the least-squares fit can be attributed to the different registration methods. Because the actual fit for each data set varies depending on other factors besides the image registration, absolute accuracy measurements are not used, instead favoring a relative comparison of each registration's results to the average from the same data set. The data sets differ in subject, level of lighting, quality of focus, number of images, and trajectory. The RMS error comparison results are shown in Figure 10.

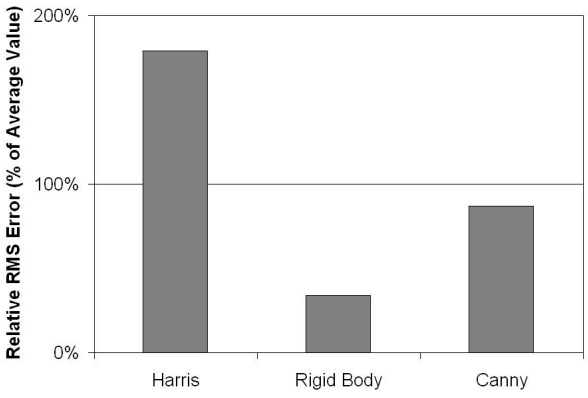

Figure 10: RMS Error Comparison of Registration Methods

The average time elapsed per image registered for each method was compared in the same manner as the accuracy. This will be important for developing real-time applications of the imaging process. The results are plotted in Figure 11.

These results show that, on the data gathered using the MLHD/Camera setup, the rigid body transform is both fastest and most successful. It provided consistently lower RMS errors while also being the least computationally extensive. Additionally, the rigid-body transformation has fewer input parameters. Thus it requires fewer adjustments from one data set to the next, as a single

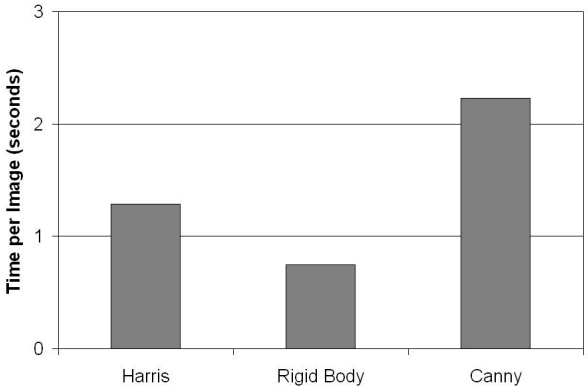

Figure 11: Running Time Comparison of Registration Methods

configuration was successful over nearly all data sets. Harris and Canny both required parameter customization for each data set as image intensities and focus changed.

Qualitatively, however, Canny is often successful in finding edges. In a situation where perspective or background are changing, a well-configured Canny algorithm should be investigated for use with registration. The time required may be prohibitive for a real-time application, however.

5 Results

5.1 Training

A plot of one test subject's training results is shown in Figure 12. In all, 1505 images were collected from this subject. The forces applied cover the force space cone in a combination of Cartesian and cylindrical grids. The RMS error in the x- and y- directions is 0.3N, 6% of the full range. The z-direction force shows an RMS error of 0.3N, 3% of the full range.

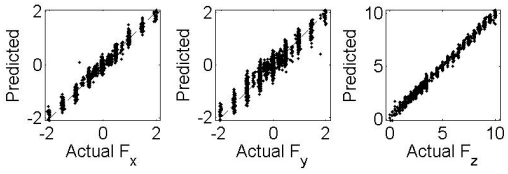

Figure 12: Subject 5's Training Results

A histogram of the training RMS error for all test subjects is shown in Figure 13. These plots have been normalized with the full range of the force, so that a distance of 0.1 on the shear plots represents 0.5N, while the same distance of the z-direction plot represents 1.0N. The errors can be seen to fall between 0-15% of the full range of forces for all subjects in all three directions.

5.2 Validation

The same test subject's validation results are shown in Figure 14. The RMS error in the shear directions is 0.3N, 6% of the full range, while the normal force has an error of 0.3N, 3% of the full range.

Figure 15 shows the RMS error histogram results for validation. Again, these plots are normalized to the full range of forces. The validation error can be seen to fall between 0-15% of the full range of forces for all three directions.

5.3 Cell Size Effects

Finally, an investigation into the effect of cell size is performed. By varying the number of cells used to represent an image of the

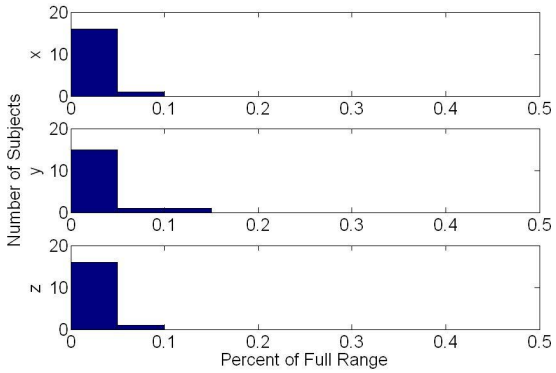

Figure 13: RMS Error of Group Training Results

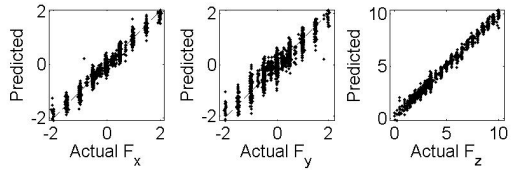

Figure 14: Subject 5's Validation Results

finger, the effect of image resolution on the accuracy of the results can be investigated. If a reduced number of cells retains the desired accuracy, it would indicate that the resolution of images in real-time applications can be reduced without loss of accuracy. It should be noted that if the number of cells is greater than the number of images, the least squares method will find an exact solution for the coefficient matrix. Thus, the training results would show 0% error. This exact solution is not useful for predicting force in additional images, as it is the equivalent of finding the exact polynomial that will fit a set of data points when what is desired is a linear best-fit line. The model would be trained to the noise in the data. For this reason, the model is restricted to a number of cells less than the number of images. The method was tested using 500, 250 and 100 cells for each image.

A sample of the training results is shown in Figure 16. A larger number of cells reduces the training error. This is to be expected, as it is the equivalent of using a higher-order polynomial to approximate a set of data.

The validation results for the same four test subjects is given in Figure 17. This shows an interesting effect. It seems that the error is slightly lower, in general, at 250 cells than it is at either 100 or 500 cells. The difference is not large, however, and the prediction error values are acceptable at every number of cells tested.

The error for all test subjects is shown in Figures 18 and 19. From these plots, it is easy to see that there is little significant difference between using 100 and 500 cells. It should be noted that reducing the number of cells from 500 to 100 results in a significant savings in computation time. For any real-time application, it will be desirable to use as few cells as possible while maintaining necessary accuracy. Thus, it is probably sufficient to use 100 cells for a real-time application.

This matches what was observed in previous work. It was demonstrated in [12] that reducing the fingernail image to 10×10 pixels did not significantly affect the accuracy of the results. Thus, in spite of increasing the complexity of the model to include arbitrary 3-dimensional force, the ability to reduce the resolution and still retain accuracy is not affected.

Another important result of this analysis is that a model trained

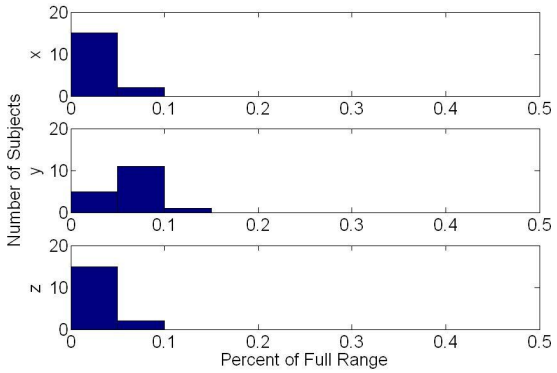

Figure 15: RMS Error of Group Validation Results

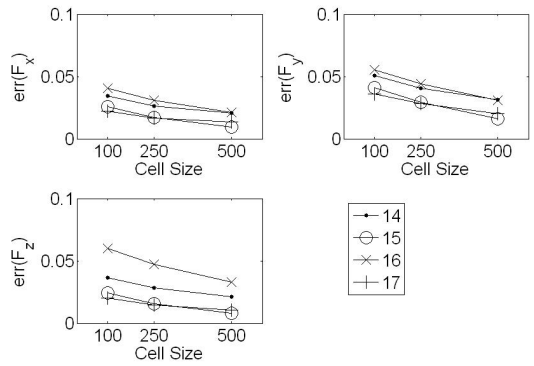

Figure 16: Effect of Cell Size on RMS Error in Training Results of Subjects 14-17

on a set of 100-cell images would not require as large a calibration data set as a model trained on a set of 500-cell images. Since there would be fewer coefficients in the low-resolution model, the calibration procedure could be performed more quickly. The current method requires 30 minutes of calibration time followed by approximately 45 minutes of data analysis. It is possible that using a calibration system with 100-cell images, the calibration time could be shortened to 10 minutes and the data analysis to 25 minutes.

5.4 Comparison to Previous Work

The validation results are compared with previous efforts in Figure 20. The first set of results, labeled Sensor, come from the original fingernail sensor developed in [7]. These include normal forces up to 3N and shear forces up to 2N. The second set, labeled Directional, comes from [11], the original fingernail imaging system. The second set of results include normal forces up to 10N and up to 2N of shear force. It should be noted that in this prior work, only one direction of force was estimated at any one time. The current work is labeled Automated. It can be seen that the automated calibration system matches or improves on the error in each force direction. Thus, despite increasing the complexity of the model to include arbitrary 3-dimensional force, the prediction accuracy improves. Figure 21 relates the same information as a percentage of the force space covered in that work.

6 Conclusion

The calibration procedure detailed herein has been shown to provide a level of accuracy matching that previously achieved. Since

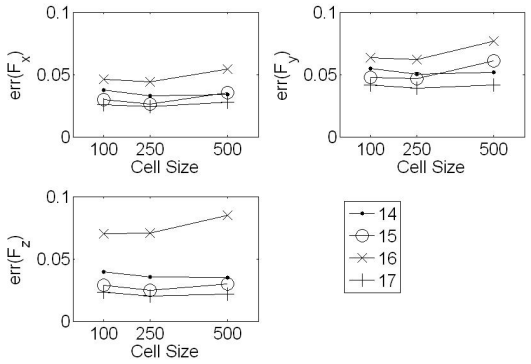

Figure 17: Effect of Cell Size on RMS Error in Validation Results of Subjects 14-17

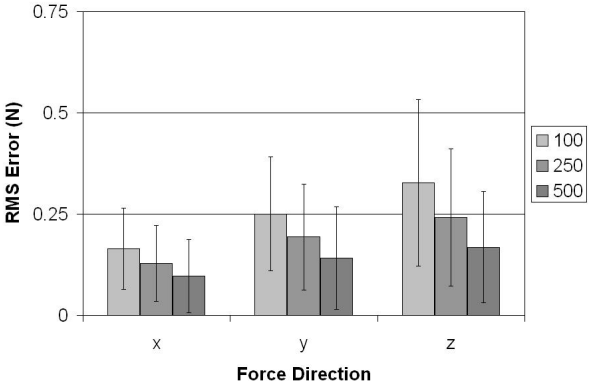

Figure 18: Effect of Cell size on RMS Error in Training Results of All Subjects

the calibration now calculates arbitrary force rather than only calculating force oriented along one axis at a time, this is an improvement on previous experiments. The shear force represented by an image is estimated to within 0.3N, or 6% of the full range of $\pm$2.5N. The normal force is estimated to within 0.3N, or 3% of the full range of 10N. Three different registration methods were compared and the rigid-body transformation method was found to provide fast, accurate results. Adjusting the number of cells used to represent the finger between 100 and 500 has been shown to have little effect on the accuracy of the measurements. This means that a real-time application could use a relatively low-resolution image of the finger. It also indicates that a relatively small data set is all that is required to perform accurate calibration. This could significantly reduce calibration and analysis time and allow a test subject to move more quickly from beginning calibration to using a demo program based on the calibration. These results could be applied to a real-time system, for example, to control the cursor on a computer screen without the need for an input device such as a mouse.

In future work, the authors desire to investigate the effects of varying contact angles, finger joint angles and shear torque on the coloration effect. The MLHD will need to be augmented to do this, as the range of motion of the flotor is insufficient. The authors plan to add a 3-DOF mechanism to the MLHD to allow for the desired range of motion. This would allow for simultaneous 3-DOF force, 1-DOF torque and 2-DOF contact angle control to determine whether these additional variables affect the accuracy of calibration.

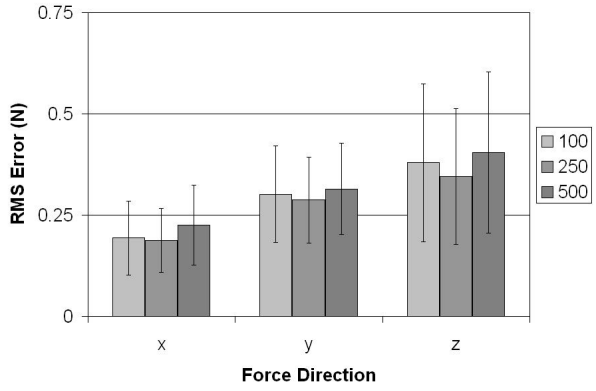

Figure 19: Effect of Cell size on RMS Error in Validation Results of All Subjects

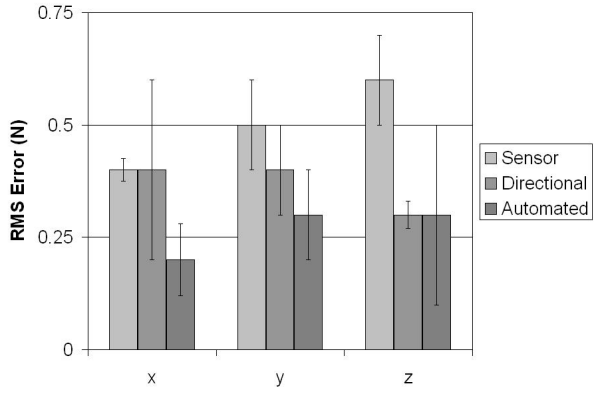

Figure 20: Comparison of Absolute Validation Error with Prior Work. Sensor data comes from [7]. Directional data comes from [11]. Current work is listed as Automated.

ACKNOWLEDGEMENTS

This work was supported by NIH Grant 1R21EB004600-01A2 and IGERT Grant DGE-0654414.

REFERENCES

[1] P. Berkelman and R. Hollis. Lorentz magnetic levitation for haptic interaction: device design, function, and integration with simulated environments. *Intl J Robotics Research*, 9:644–667, 2000.

[2] A. Brown. A survey of image registration techniques. *ACM Computing Surveys*, 24:226–276, 1992.

[3] J. Canny. A computational approach to edge detection. *IEEE Transactions on Pattern Analysis and Machine Intelligence*, PAMI-8(6):679–698, 1986.

[4] M. A. Fischler and R. Bolles. Random sample consensus: a paradigm for model fitting with applications to image analysis and automated cartography. *Communications of the ACM*, 24(6):381–395, jun 1981.

[5] T. Grieve, Y. Sun, J. Hollerbach, and S. Mascaro. 3-d force control on the human fingerpad using a magnetic levitation device for fingernail imaging calibration. In *World Haptics*, pages 411–416, 2009.

[6] C. Harris and M. Stephens. A combined corner and edge detector. In *Proceedings Fourth Alvey Vision Conference*, pages 147–151, 1988.

[7] S. Mascaro and H. Asada. Photoplethysmograph fingernail sensors for measuring finger forces without haptic obstruction. *IEEE Transactions on Robotics and Automation*, 17(5):698–708, 2001.

[8] S. Mascaro and H. Asada. The common patterns of blood perfusion in the fingernail bed subject to fingertip touch force and finger pos-

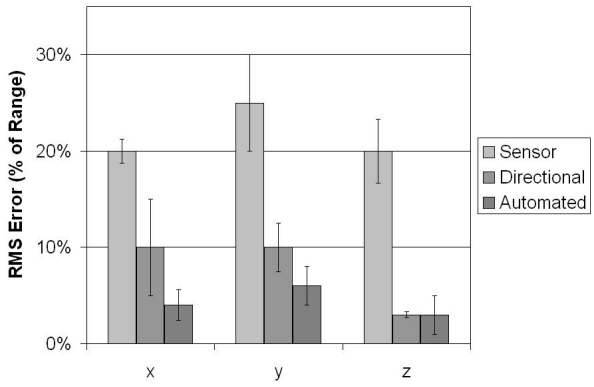

Figure 21: Comparison of Relative Validation Error with Prior Work. Sensor data comes from [7]. Directional data comes from [11]. Current work is listed as Automated.

ture. *Haptics-e: The Electronic Journal of Haptics Research*, 4(3):1–6, 2006.

[9] S. Mascaro and H. H. Asada. Measurement of finger posture and three-axis fingertip touch force using fingernail sensors. *IEEE Trans. on Robotics and Automation*, 20:26–35, 2004.

[10] Sciavicco and Siciliano. *Modeling and Control of Robot Manipulators*. London; New York: Springer, 2000.

[11] Y. Sun, J. M. Hollerbach, and S. A. Mascaro. Measuring fingertip forces by imaging the fingernail. In *Proc. 14th Symposium on Haptic Interfaces for Virtual Environment and Teleoperator Systems*, pages 125–131, 2006.

[12] Y. Sun, J. M. Hollerbach, and S. A. Mascaro. Eigennail for finger force direction recognition. In *Proc. IEEE Intl. Conf. Robotics and Automation*, pages 3251–3256, 2007.

[13] Y. Sun, J. M. Hollerbach, and S. A. Mascaro. Predicting fingertip forces by imaging coloration changes in the fingernail and surrounding skin. *IEEE Trans. on Biomedical Engineering*, 55(10):2363–2371, 2008.

[14] Y. Sun, J. M. Hollerbach, and S. A. Mascaro. Finger force direction estimation with computer vision. *IEEE Transactions on Robotics*, In Press.